ELECTROKINETIC SOUNDING METHOD TO MAP HYDROGEOLOGICAL BOUNDARIES

Mohammad S. Rosid & Anton W. Kepic

CRC LEME, Department of Exploration Geophysics, Curtin University of Technology, PO Box U1987, Perth, WA, 6845

INTRODUCTION

Despite steady progress in the understanding of electrokinetic or seismoelectric processes over the years, further field studies are needed to develop acquisition methodology as well as processing for testing the electrokinetic (EKS) method's viability. Many past studies appear to be opportunistic rather than controlled tests. Very few of the researchers cited have published more than one example of field data, and generally these reports show electrokinetic signals from only one layer (water table or weathered base), e.g., glacial till interface. This may be blamed upon the very weak signals (μV/m to mV/m) that are extremely difficult to measure, and also a lack of predictive theory to design experiments to test hypotheses.

The electrokinetic effect is a seismic-to-electromagnetic coupling mechanism that results from a coupling between fluid flow and electric current flow in a medium containing both solid and liquid components. It is similar to the phenomenon of streaming potential (electric) arising from the movement of groundwater. A charge distribution known as the electrical double layer exists at solid-liquid interfaces within the rock matrix. The electrokinetic effect arises because only part of the electrical double layer is free to move within the liquid relative to the solid. Thus, small-scale motions of fluid relative to the solid matrix induced by seismic P-waves lead to small-scale electric currents, which can result in macroscopic polarization and electric fields.

Many factors influence the electrokinetic responses measured in the field. The signals are strongly dependant on at least three main physical properties: porosity of rock; permeability; and, fluid-chemistry. In theory, there is little or no seismoelectric response in partially or unsaturated media (Zhu & Toksoz 2003) so the geological medium must be saturated by an electrolyte. The permeability, as reported by Jouniaux & Pozzi (1995), has a strong influence on streaming potentials when the fluid is very resistive, and hence affects the electrokinetic response as these effects are related. The salinity of groundwater, as an electrokinetic parameter, has strong correlation to the seismoelectric response, in which the largest streaming potential is associated with fresh fluid environments (Revil *et al.* 1996). Furthermore, electrokinetic signals are divided into two types (Butler *et al.* 1996, Haartsen & Pride 1997). The first type of signal is a non-radiating field, which occurs in homogenous media, and is contained within and travels with the seismic P-wave. The second type of signal is raised when the P-wave passes through a boundary with contrast in elastic and/or electrokinetic (fluid-chemistry) properties. The electric signals diffuse rapidly to the sensors with an apparent velocity that is much faster than any seismic wave. Thus, the signals will arrive nearly simultaneously across an array of widely spaced dipole sensors. The second type are the signals that can be used to determine hydrogelogical properties.

Figure 1: Borehole log showing gamma ray, geological, and induction logs (from left to right). It is predominately sand/sand-clay mixtures. These layers overlay alluvial sediments until a saprolite granite bedrock boundary is reached. The log data also shows that the induction and gamma logs indicate more structure than the geological log.

GEOLOGY AND HYDROGEOLOGY OF AREA

The EKS survey described in this paper was done in a semi-arid area, with little or no topography, near the town of Pingrup (Lake Grace), Western Australia. The location is north of Pingrup, approximately 400 km southeast of Perth. The area is characterized by low permeability due to the silty and clayey nature of the regolith. However, sandy intervals with intergranular porosity and the alluvium are significant as local aquifers and a source of groundwater for watering farm stock (Dodson 1999).

A geological and geophysical log (Figure 1) from a borehole, 2 m away from the EKS acquisition line, shows an example of the lithology in the test area. There are four main specific layers: (i) alluvial sands and clays layer up to 18 m thick; (ii) carboneous sand up to 14 m thick; (iii) a great silty sand layer up to 23 m thick; and,

(iv) saprolite granite bedrock. In detail the figure shows the alluvial sand layers as being interbeded by thin clay layers as well as peaty sand and silty sand. These boundaries may have contrasts in permeability, electrokinetic or elastic properties, which may influence to change the characteristic of both seismic and seismoelectric waves when they pass through.

Chemically, the groundwater pH is slightly acidic, with a pH range from 3 to 7. Sodium and chloride are the most dominant ions in groundwater in this area, with the source of the sodium and chloride due to accumulation of salt carried by rainfall (Hingston & Gailitis 1976). In general, the groundwater in this area is predominantly saline to hypersaline, ranging from less than 1,000 mg/L TDS (total dissolved solid) to more than 35,000 mg/L TDS, with a maximum resistivity of the order of 5 ohm-m. Low-salinity groundwater may be located within the first few meters of the water table within sandy surficial sediments; the salinity will tend to increase dramatically with depth (Dodson 1999). The water table at that time of the survey was at approximately 5 m depth, situated within a clayey sand interval. The main aquifer appears to be a relatively thick sand unit that overlays the saprolite/granite bedrock. This unit appears to be part of the paleochannel sediments.

METHODOLOGY

Our main field instrumentation consisted of a 24-channel seismograph (OYO DAS1) equipped with a roll box, CDP cables and single, 30 Hz vertical component geophones and electric sensors. The electric field sensors were grounded dipoles, each consisting of a pair of 50 cm long stainless steel stakes. The stakes were driven approximately to 30 cm depth into the ground, and paired to form 5 m dipoles with the positive electrodes are inward direction of array. The dipoles were arranged in a staggered array in the direction of the profile to improve the quality of data. Each dipole was connected, via wire leads, to a battery-powered differential preamplifier located half-way between stakes. The amplified signals are then transmitted along conventional seismic reflection cables to the recorder. To avoid electrical cross-contamination, seismic and seismoelectric data were not recorded simultaneously. The preamplifiers provided an electronic gain of 30. Meanwhile, seismic excitation was provided by a sledgehammer onto a plastic-aluminum base plate. 30 to 50 hammer blows are stacked to produce a seismoelectric record in order to achieve an acceptable S/N ratio. Only 10 hammer blows were used for stacking seismic data.

To cancel the regional electrical noise, and enhance the signal, a symmetric split spread configuration of twenty-four dipole sensors were set in-field. Twenty-four of geophones and twenty-four of grounded dipoles were set at 2 m and 25 cm or 50 cm intervals, respectively, to prevent spatially aliased data of the first type of electrokinetic signal. In addition, to improve the electrokinetic signals the dipole array was arranged in an overlapping configuration.

RESULTS

The seismic refraction data (Figure 2) were processed using the time-intercept method to provide P-wave velocities and layer dips and depths (Palmer 1986, Burger 1992). Four near-surface layers were identified. These layers may be attributable to: unsaturated alluvial sand-sandy clay; a semi-saturated alluvial clayey sand layer; saturated sedimentary sand; and, a saturated peaty sand layer. The apparent velocities are 690 m/s, 1260 m/s, 1990 m/s, and 2400 m/s, respectively. The layers are almost flat with thicknesses of 2 m, 4 m, and 9 m respectively.

Figure 3 displays examples of raw electric-field data (shot records) recorded at two different locations in the Lake Bryde area. The data, in which a 90 µV maximum amplitude signals, has been processed using the sinusoidal subtraction technique (Butler & Russell 1993) to remove low amplitude powerline noise. The section is dominated by electrical signals associated with ground-roll. This signal masks other electrical signals from the direct P-wave, refraction's near the electrodes, and electrokinetic signals from interfaces. Dipoles nearest to the shot-point are most affected, however, the presence of electric signals associated with compression head wave are also be visible as first arrivals on the near-offset traces. Signals from dipoles with greater offset display higher apparent velocity that can be attributed to direct P-wave or refraction's near the electrodes.

The only simultaneous events visible in the raw records are related to the trigger signal or from telluric noise (visible at later times in Figure 3). In general, the polarity of this type of signal is reversed on opposite sides of the shotpoint. Simultaneous seismoelectric signals (the second type of electrokinetic signal described previously) only becomes evident (Figure 4) after implementing a (50 – 55 – 600 – 650 Hz Ormsby zero phase) band-pass filter and followed by other 200 – 600 Hz Butterworth zero phase band pass filter to remove some low frequency signals. The filtered shot records in Figure 4 show that a series of high-

frequency events have reached all dipoles at approximately the same time, and are most evident and consistent at early times. The three shot records above are from the same location and same electrode configuration.
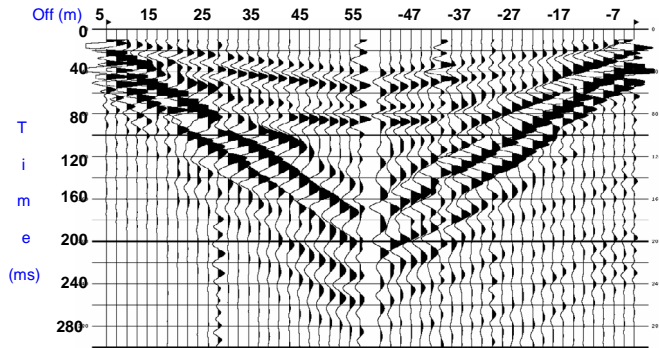
Figure 2: The seismic shot records from two different shot points which are 5 m away from 1st and 26th geophone for left and right hand, respectively. The data are quite similar and symmetrical. The time trigger is on 10 ms.
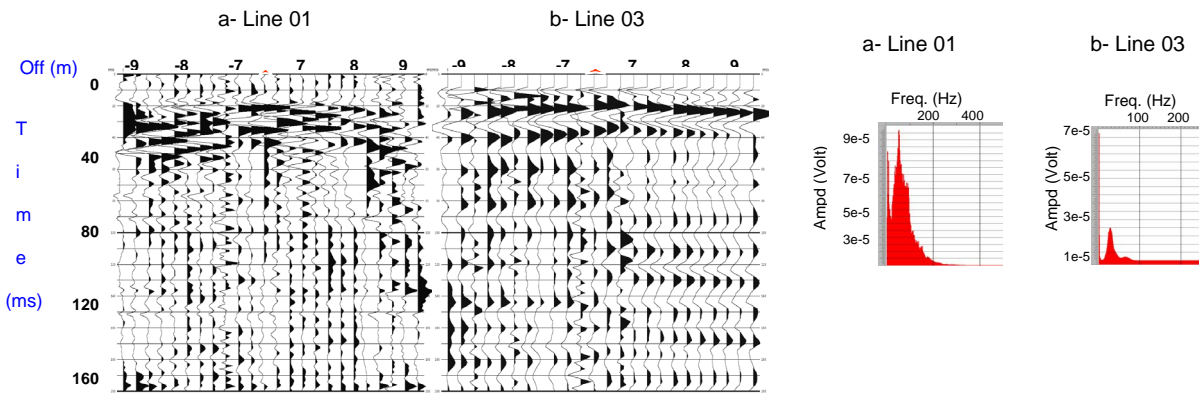
Figure 3: Seismoelectric shot records recorded by 24 dipoles with a dipole sensor spacing of 25 cm for both lines. The data was obtained by stacking 30 to 50 hammer blows with a split spread and overlapping dipole configuration. The spectrum amplitudes are shown on the right side, where the maximum amplitude is around 90 µV at line 01.
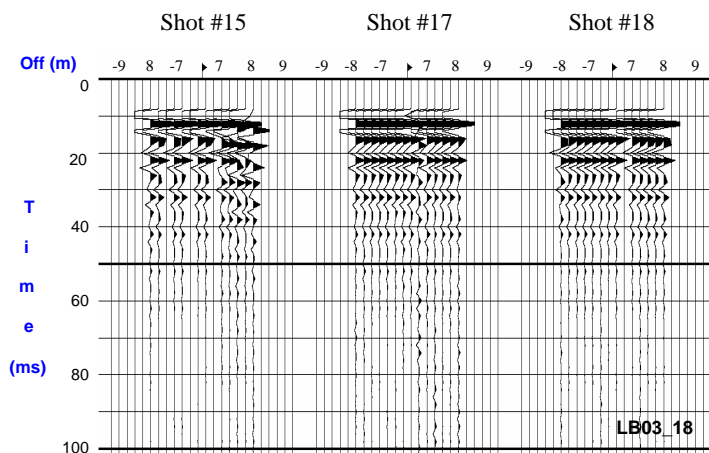
Figure 4: The electrokinetic data from line 03 with three different shots after applying a 200 – 600 Hz Butterworth zero phase band-pass filter. Note that time at impact (trigger) is at 10 ms. Simultaneous signals are evident at 11, 15.5, 21, 23, 25, 28, 31, 36 and 41 ms. Other later signals are not truly simultaneous.

The ability to reproduce these signals provides us with confidence that they arise from geological boundaries. Most of the later signals recorded at this location are interpreted to be noise as they are not consistently reproduced. As a further check of the validity of an event being simultaneous a careful check of the apparent velocity is made (on an enlarged portion of the shot record). Figure 5 displays some of the filtered data in Figure 4 over the interval 5-45 ms.
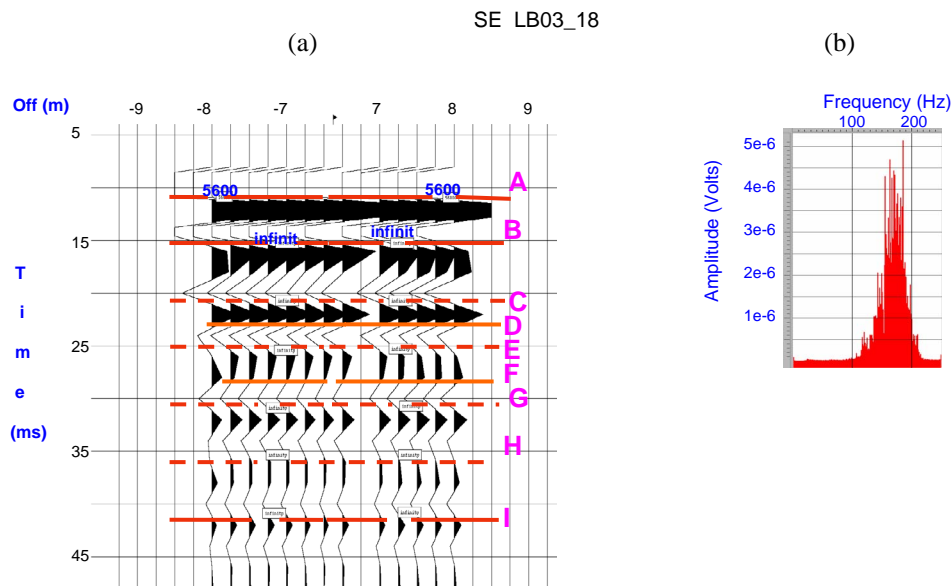
Figure 5. (a). Enlarged view of shot #18 record shown in Figure 3 showing simultaneous signals from interfaces. Bold lines and dashed lines associated with geological and geophysical changing, respectively. (b). Its average amplitude spectrum with automatic gain control (AGC).

There are nine particular events in Figure 5, labeled A through I arriving 1.1 ms, 5.5 ms, 11 ms, 13.2 ms, 15.4 ms, 18.3 ms, 21.2 ms, 25.8 ms and 31 ms after impact, that are truly simultaneous and are interpreted to be electrokinetic signals from interfaces. The A event has strongest electric amplitude due to its proximity to the surface (earlier arrival time). The measured apparent velocity of 56,000 m/s for signals A and very large (infinity) velocity for other signals are within the expected velocity range of an EM disturbances in a moderately conductive medium. The very saline nature of the area, of the order of 0.3 to 5 ohm-m for the first 50 m, may play a significant role to the amplitude spectrum in range of micro to nano-Volts (Figure 5b).

The geological log and seismic refraction data were used to locate the depth of the interfaces and the likely geological feature causing the events identified in Figure 5. The events A, through I are calculated from the refraction velocities to have come from depths of 1 m, 5 m, 11 m, 18.5 m, 21 m, 32 m, 37 m, 45 m, and 55 m respectively. Five events, A, B, D, F, and I, are associated with geological change, whereas events, C, E, G, and H, have a strong correlation with physical property changes. Events A and B appear to originate from the density contrast between the unsaturated alluvial sandy clay and sand layers and fluid chemistry contrast at the water table at 1m and 5m depths, respectively. Events D, F, and I appear to originate from the alluvial sand to peaty sand boundary, peaty sand to silty sand boundary, and silty sand to granite basement at 18 m, 32 m, and 55 m depths, respectively. Events A and B are most likely generated by a boundary which has a contrast in impedance and water salinity, respectively. While events D, F, and I are caused by boundaries having an impedance contrast. Events D and F have negative polarization that might be due to passing of the P-wave from a permeable to a relatively impermeable layer. These boundaries generally increase in clay content as shown at gamma log data. Events C, E, G, and H, cannot be explained by the geological log. However, an examination of the gamma and induction logs may account for these physical changes. Event C might be associated with the drop of clay content at 11 m. Event E is likely to be associated with a thin layer of high conductivity within the peaty sand column at 21 m depth. The driller's field log describes changes in porosity at around 22 m depth from black peaty loam to black peaty fine-medium sand. Larger porosity leads to a thicker double layer, and may provide a larger streaming potential. While events G and H appears associated with a small change of clay content within the silty sand unit at 37 m and 45 m depth, respectively. According to the detail of driller's log, however, these events might also be caused by the changing of granular size of silty sand, from sub rounded to coarse silty sand and from coarse to medium silty sand for G

and H, respectively. We believe that events C, E, G, and H are most likely due to porosity and permeability changes rather than water salinity changes. Analysis shows that electrokinetic negative polarity may be caused by a boundary with increasing clay content. Clay is a major contributor to rock cementation process, which may lead to form an impermeable rock. So, the negative polarity of electrokinetic signal is most likely caused by a boundary between a permeable and a relatively impermeable layer, and vice versa.

CONCLUSIONS

We have verified experimentally the existence of two electrokinetic effects: an electric field that accompanies the seismic wave and EM signals generated at depth from geological boundaries which have contrasts in either seismic or electro-chemical properties. Electrokinetic signals from at least three boundaries up to depths of 55 m in conductive ground were identified, and shown to be related to formations visible in geological and geophysical well-logs. The negative polarity of the electrokinetic signal is most likely associated with either a boundary with increasing clay content (which may affect rock cementation), or a boundary of a permeable to a relatively impermeable layer. This provides significant hope that the electrokinetic method may be able to be used in groundwater exploration in the future to detect significant hydro-geological changes before drilling. However, for further work in improving survey design is still needed to reduce electronic and natural noise as well as better processing methods to attenuate coherent noise.

REFERENCES

BURGER H.R. 1992. *Exploration Geophysics of the shallow subsurface*, Prentice Hall, New Jersey, pp. 80-96.

BUTLER K.E., RUSSELL R.D., KEPIC A.W. & MAXWELL M. 1996. Measurement of the seismoelectric response from a shallow boundary. *Geophysics* **61**, 1769-1778.

BUTLER K.E. & RUSSELL R.D. 1993. Subtraction of powerline noise from geophysical records. *Geophysics* **58**, 898-903.

DODSON W.J. 1999. *Hydrogeology of the Newdegate 1:250 000 sheet: Water and Rivers Commission*, Hydrogeological Map Explanatory Notes Series **Report HM 5**, 27p.

HAARTSEN M.W. & PRIDE S.R. 1997. Electroseismic waves from point sources in layered media. *J. Geophysical Research* **102**, 24745-24769.

HINGSTON F.J. & GAILITIS V. 1976. The geographic variation of salt precipitated over Western Australia. *Australian Journal of Soil Research* **14**, 319-335.

JOUNIAUX J. & POZZI J. 1995. Streaming potential and permeability of saturated sandstones under triaxial stress: Consequences for electrotelluric anomalies prior to earthquakes. *J. Geophysical Research* **100**, 10197-10209.

PALMER D. 1986. Refraction Seismic, the lateral resolution of structure and seismic velocity. *In:* HELBIG K. & TREITEL S. eds. *Handbook of geophysical exploration: section I. Seismic Exploration.* Geophysical Press, London, 30-46.

REVIL A., DAROT M. & PEZARD P.A. 1996. From surface electrical properties to spontaneous potentials in porous media. *Surv. Geophysics* **17**, 331-346.

ZHU ZHENYA & TOKSOZ M.N. 2003. Seismoelectric measurements in cross-borehole models with fractures. *Proceedings of the 6th SEGJ International Symposium*, Tokyo, Japan, 342-347.